Translational Imaging of the Fibroblast Activation Protein (FAP) Using the New Ligand [^{68}Ga]Ga-OncoFAP-DOTAGA

Philipp Backhaus (✉ philipp.backhaus@ukmuenster.de)

University Hospital Münster   https://orcid.org/0000-0003-4164-4104

Florian Gierse

University of Münster, European Institute for Molecular Imaging

M.C. Burg

University Hospital Münster, Clinic for Radiology

Florian Büther

University Hospital Münster, Department of Nuclear Medicine

Inga Asmus

University Hospital Münster, Department of Nuclear Medicine

Paulina Marie Dorten

University of Münster, European Institute for Molecular Imaging

Juela Cufe

University Hospital Münster, Department of Nuclear Medicine

Wolfgang Roll

University Hospital Münster, Department of Nuclear Medicine

Dario Neri

Philogen SpA

Samuele Cazzamalli

Philochem AG

Jacopo Millul

Philochem AG

Jacqueline Mock

Philochem AG

Andrea Galbiati

Philochem AG

Aureliano Zana

Philochem AG

Klaus P. Schäfers

European Institute for Moleuclar Imaging, University of Münster

Sven Hermann

European Institute for Molecular Imaging, University of Münster

Matthias Weckesser

University Hospital Münster, Department of Nuclear Medicine

Joke Tio

University Hospital Münster, Department of Gynecology & Obstetrics

Stefan Wagner

University Hospital Münster, Department of Nuclear Medicine

Hans-Jörg Breyholz

University Hospital Münster, Department of Nuclear Medicine

Michael Schäfers

University Hospital Münster, Department of Nuclear Medicine

Abstract

Purpose

The fibroblast activation protein (FAP) is an emerging target for molecular imaging and therapy in cancer. OncoFAP is a novel small organic ligand for FAP with very high affinity. In this translational study, we establish [^{68}Ga]Ga-OncoFAP-DOTAGA (^{68}Ga-OncoFAP) radiolabeling, benchmark its properties in preclinical imaging and evaluate its application in clinical PET scanning.

Methods

^{68}Ga-OncoFAP was synthesized in a cassette-based fully automated labelling module. Lipophilicity, affinity, and serum stability of ^{68}Ga-OncoFAP were assessed by determining log$D$7.4, IC$_{50}$ values and radiochemical purity. ^{68}Ga-OncoFAP tumor uptake and imaging properties were assessed in preclinical dynamic PET/MRI in murine subcutaneous tumor models. Finally, biodistribution and uptake in a variety of tumor types were analyzed in 12 patients based on individual clinical indications that received 163 ± 50 MBq ^{68}Ga-OncoFAP combined with PET/CT and PET/MRI.

Results

^{68}Ga-OncoFAP radiosynthesis was accomplished with high radiochemical yields. Affinity for FAP, lipophilicity and stability of ^{68}Ga-OncoFAP measured are ideally suited for PET imaging. PET and gamma counting-based biodistribution demonstrated beneficial tracer kinetics and high uptake in murine FAP expressing tumor models with high tumor-to-blood ratios of 8.6 ± 5.1 at 1 h and 38.1 ± 33.1 at 3 h p.i. Clinical ^{68}Ga-OncoFAP PET/CT and PET/MRI demonstrated favorable biodistribution and kinetics with high and reliable uptake in primary cancers (SUV$_{max}$ 12.3 ± 2.3), lymph nodes (SUV$_{max}$ 9.7 ± 8.3) and distant metastases (SUV$_{max}$ up to 20.0).

Conclusion

Excellent preclinical and clinical imaging characteristics validate ^{68}Ga-OncoFAP as a powerful alternative to currently available FAP tracers.

Introduction

The fibroblast activation protein (FAP) is a membrane serine protease expressed by fibroblasts. FAP has recently emerged as one of the most promising target structures for molecular imaging and therapy in cancer [1, 2]. In contrast to the ubiquitous presence of non-FAP expressing quiescent fibroblasts, FAP expression by activated fibroblasts in the adult is (with few exceptions) linked to pathologic states such as wound healing, organ fibrosis and cancer, where it is abundantly expressed by cancer-associated fibroblasts (CAFs) in the tumor microenvironment [3].

Radiolabeled FAP-targeting small ligands based on FAP inhibitors (FAPI) have recently been introduced and demonstrated very promising characteristics for PET imaging such as high and fast uptake in a variety of cancers and rapid clearance from the majority of healthy organs [4–6]. As of now, a growing body of clinical studies have established a high versatility of FAPI-PET to detect the spread of a wide range of cancers. Importantly, FAPI-PET seems to be able to fill clinically urging shortcomings of ^{18}F-FDG, for example in pancreatic cancer [7], primary liver tumors [8], gastric and bowel cancer [9] and breast cancer [10].

In addition to its role in diagnostic imaging, reliable expression in cancer and wide absence in other tissues potentially qualify FAP as a theranostic molecular target. Radioligand therapy using α- or β-emitting isotopes appears tempting, in light of recent break through clinical studies of theranostic agents targeting somatostatin receptors in neuroendocrine tumors [11] and prostate-specific membrane antigen (PSMA) in prostate cancer [12]. However, first published retrospective studies on clinical radioligand therapy with FAPI agents leave open questions regarding their therapeutic efficacy [13, 14]. In addition, targeted delivery of non-radioactive drugs and chimeric antigen receptor (CAR) T-cells have been discussed to employ FAP for targeted molecular therapy [15]. For all of such therapeutic approaches, FAP-targeted molecular imaging will play an indispensable role to stratify patients.

A variety of specific FAP radioligands have been introduced, of which the ligands initially developed at the University of Heidelberg, i.e. FAPI-04 [6] and FAPI-46 [16] are most abundantly and very successfully used in published PET imaging studies. Recently, the new very high-affinity FAP ligand OncoFAP was shown to possess selective FAP binding *in vitro* and striking tumor uptake in animal models after ^{177}Lu or fluorophore labelling [15]. In this translational study, we describe the radiosynthesis of [^{68}Ga]Ga-OncoFAP-DOTAGA (^{68}Ga-OncoFAP), its preclinical evaluation in murine tumor models and results from first clinical application of ^{68}Ga-OncoFAP in different cancers.

Material And Methods

Radiosynthesis, *in vitro* tests and assays

^{68}Ga-FAPI-46 was synthesized as described previously [10]. FAPI-46 precursor for preclinical and clinical imaging was kindly provided under a MTA by U. Haberkorn (Heidelberg, Germany). OncoFAP-DOTAGA was synthesized as previously reported [14]. Radiolabeling was performed on the basis of the German Pharmaceuticals Act (AMG §13 (2b)), i. e. magistral preparation. Briefly, radiogallium ($T_{1/2}$=68 min, β^+ = 89 % and EC=11 %) was automatically eluted with 0.1 M HCl (0.36%) from a 50 mCi (1.85 GBq) ^{68}Ge/^{68}Ga radionuclide generator (EZAG, Berlin, Germany) without pre-purification of the eluate and transferred into the reaction vessel of the ^{68}Ga-radiosynthesis module. Two types of single use disposable-cassette-based modules, either a manual iQS Ga-68 Fluidic Labeling Module (itG, Garching, Germany) or a fully automated labeling module (miniAllinOne, Trasis, Ans, Belgium), containing a pre-heated, buffered OncoFAP-DOTAGA solution, were used for radiolabeling. After incubation for a few minutes at ca. 100°C,

the reaction mixture was loaded onto a SPE cartridge, eluted with EtOH in the product vial and formulated with additional 0.9% NaCl. For clinical imaging, a full QC was performed for each preparation of ^{68}Ga-OncoFAP. All QC parameters (see Suppl. Table 1) were in accordance with the Ph. Eur. standards for ^{68}Ga-DOTA-TOC (monograph 2482). For preclinical imaging, a restricted QC was performed and ^{68}Ga-OncoFAP or ^{68}Ga-FAPI-46 product solutions were subsequently concentrated by rotary evaporation under reduced pressure to remove the ethanol and redissolved in a small volume of physiological saline, suitable for injection into mice.

The metabolic stability of ^{68}Ga-OncoFAP was assessed after incubation with human and mouse blood serum at 37°C by analytical radio-HPLC performed at different time points after incubation (i.e., 30, 60, 90, and 120 min).

The lipophilicity of ^{68}Ga-OncoFAP-DOTAGA was determined according to previously described procedures [17].

Enzymatic inhibition activity and selectivity of OncoFAP derivatives was assessed by employing commercially available *in vitro* fluorescence assays for FAP, dipeptidyl peptidase 8 (DDP8) and prolyl oligo peptidase (POP) (BPS Bioscience, San Diego, CA, US). The fluorogenic substrate (Fluorogenic DPP substrate 1, Ala-Pro-AMC dipeptide, AMC: 7-Amino-4-methylcumaryl-) was incubated together with recombinant FAP, DDP or POP/PREP in the presence or absence of test compounds. The enzymatic activity was correlated with the amount of cleaved fluorescent product measured by fluorescence spectroscopy. IC_{50} of each test compound was determined from the curves obtained by plotting fluorescence intensities at different concentrations of the inhibitor.

More detailed information is provided in the supplementary material.

Animal studies

All experiments were conducted in accordance with the German Law on the Care and Use of Laboratory Animals and approved by the Landesamt für Natur, Umwelt und Verbraucherschutz of North Rhine-Westphalia, Germany.

For tumor-xenograft models, female NMRI nu/nu mice (Janvier, France), 8 - 9 weeks old, were housed at a constant temperature (22°C) and relative humidity (40 % - 55 %) under a regular light/dark schedule. Food and water were available ad libitum.

Tumor cells (10^6 cells in 50 µl saline) were implanted subcutaneously in the shoulders of NMRI mice with HT1080 wildtype (FAP-) in one shoulder and with stably transfected human FAP-expressing HT1080 cells (FAP+) in the contralateral shoulder. Cells were kindly provided by U. Haberkorn, University of Heidelberg [5]. At day 11 after implantation, mice received whole-body PET/MRI (1 T Mediso nanoScan) imaging with list mode PET for 60 minutes and additional non-contrast-enhanced anatomic, coronal T1-weighted MRI, followed by late static PET/MRI imaging 180 min p.i. Either ^{68}Ga-OncoFAP or ^{68}Ga-FAPI-46

(n=6 each) were injected into the tail vein with a syringe pump at 1000 µL/min in a volume of 100 µL 30 seconds after the start of PET. At the next day (day 12 after implantation), the same mice were injected with the respective other FAP-tracer and received identical dynamic PET/MRI for 60 minutes. 60 minutes p.i., mice were sacrificed under deep narcosis and organs and body fluids were harvested, weighed and γ-counted. All involved measuring hardware (dose calibrator ISOMED 2010, automatic γ-counter PERKIN ELMER WALAC 2480, Twilite coincidence detector Swisstrace, PET/MRI) were cross-calibrated for ^{68}Ga. Overall, 3 scans were rejected, because of extravasation (day 11 OncoFAP), inability of i.v. access (day 12 FAPI-46) and insufficient radioactivity (day 12 FAPI-46), respectively. The resulting injected amounts of radioactivity for the remaining 11 ^{68}Ga-OncoFAP scans and 10 ^{68}Ga-FAPI-46 scans were 19.2 ± 4.4 MBq and 18.2 ± 4.8 MBq, respectively.

Dynamic PET scans were reconstructed in time frames of 1 x 30 s, 5 x 12 s, 5 x 60 s, 4 x 300 s, 2 x 600 s and 1 x 810 s. Frames 12, 18 and the late scan are referred to as (rounded) 10 min, 1 h and 3 h throughout the manuscript. Volume of interests (VOI) of tumors and representative organs were defined on anatomic MRI. Resulting tumor volumes for ^{68}Ga-OncoFAP scans for FAP+ and FAP- tumors were 0.4 ± 0.36 and 0.22 ± 0.15; for FAPI-46 scans 0.34 ± 0.20 and 0.2 ± 0.17 (n.s. different between the two tracers).

Preclinical pharmacokinetic modelling

Before PET/MRI at day 12 p.i. mice received surgery to establish an extracorporeal circulation shunting the blood from the femoral artery to the tail vein or contralateral femoral vein as described previously [18]. At 40 cm from the femoral artery the shunt (0.3 mm inner diameter silicon; total extracorporeal volume 56.6 µl) was led through a Twilite coincidence detector. Acquired blood activity curves were calibrated with a separately measured calibration factor for ^{68}Ga according to vendors instructions. The curves were corrected for delay and dispersion based on a numerical deconvolution, using dispersion kernels derived from measuring step functions at defined pumping speeds. Standard 2-tissue compartmental (2TCM) pharmacokinetic (PK-) modelling and Patlak analysis was performed for the triceps muscle, FAP- and FAP+ tumors using PMOD version 3.703 (PMOD Technologies LLC) and was based on mean PET VOI time-activity curves and Twilite-based extracorporeal arterial input functions (AIF). AIF plasma fraction was calculated based on direct hematocrit measurements after imaging (StatStrip® Hb/Hct, Nova Biomedical).

Patients

We retrospectively analyzed ^{68}Ga-OncoFAP PET/CT and PET/MRI scans of 12 patients. Primary tumors were breast cancer in 8 patients. The other 4 patients had fibrosarcoma, colon cancer, hepatocellular carcinoma and an unclear cystic pancreatic tumor, respectively. Patients were referred by their treating oncologist on an individual clinical basis to support initial staging or specific diagnostic challenges in relapsed cancer. All patients gave written informed consent for ^{68}Ga-OncoFAP-PET/MRI and/or PET/CT imaging and retrospective scientific analysis. Analysis has been approved by the Ethics Committee of the

Medical Association of Westphalia-Lippe and the Medical Faculty of the University of Münster (Az. 2021-408-f-S). This study includes all ^{68}Ga-OncoFAP-PET/CT and PET/MRI scans conducted at the University Hospital Münster 01-06/2021. No exclusion criteria were applied.

Clinical PET/CT and PET/MRI

Patients were injected with 163.3 ± 50 MBq ^{68}Ga-OncoFAP. Patient were scanned in supine whole-body PET/CT (mCT, Siemens Healthineers) or PET/MRI (mMR, Siemens Healthineers) ~ 1 h p.i. as described previously [10]. Breast cancer patients additionally received prone breast PET/MRI before the whole-body scan ~30 min p.i. and subsequent diagnostic contrast-enhanced CT or MRI was added according to the specific clinical demand, see Table 3 for details. One patient underwent dynamic imaging initiated with tracer injection in PET/CT, consisting of list mode PET of a mediastinal field of view for 2 minutes (reconstructed frames 6 x 10 s, 3 x 20 s) and subsequent whole-body dynamic scanning consisting of 6 bed positions that were scanned 7 x 45 s from the skull base to mid-thighs. Eventually, 40 min p.i. a whole-body scan with 3 minute per bed positions was acquired. Reading of PET/MRI and PET/CT was performed according to a standard clinical workflow. Standard uptake values (SUV) measurements were acquired in Syngovia (Siemens Healthineers) with circular or spherical volumes of interests.

Statistics

Statistical analysis was performed using Matlab (R2020a, Mathworks). Mann-Whitney-U tests were performed for pairwise comparisons. p values <.05 were considered statistically significant. If needed, Bonferroni correction was applied to account for multiple testing. All values are displayed as mean ± std if not stated otherwise.

Results

Radiosynthesis, *in vitro* tests and assays

OncoFAP-DOTAGA was synthesized as shown in Scheme 1 [14]. ^{68}Ga-OncoFAP was prepared using a manual and a fully automated synthesis module with a radiochemical yield (rcy) of 69.1 ± 12.7 % and 75.3 ± 2.9 % and radiochemical purity (rcp) of 97.5 ± 1.1 % and 98.1 ± 1.1 %, respectively (n=16 for each module). All QC parameters were in accordance with the Ph. Eur. standards given for ^{68}Ga-DOTA-TOC and thus syntheses on both modules were suitable for application in the clinics (for details see Suppl. Table 1). The non-radioactive tracer analogs [^{nat}Ga]Ga-OncoFAP-DOTAGA (^{nat}Ga-OncoFAP) and [^{nat}Ga]Ga-FAPI-46 (^{nat}Ga-FAPI-46) were synthesized as described in the supplemental material.

Stability of ^{68}Ga-OncoFAP was assessed by radio-HPLC chromatograms after incubation in serum (Fig. 1 for human serum, Suppl. Fig. 3 for mouse serum). As a result, ^{68}Ga-OncoFAP shows metabolic stability in murine as well as human blood serum for at least 120 min.

The experimental Log$D$7.4 value was -3.91 ± 0.32 (n=6). Thus, ^{68}Ga-OncoFAP can be considered to be highly hydrophilic, which should be advantageous for imaging application since renal excretion route is favored and low background can be obtained.

We assessed the enzymatic inhibition activity of [nat]Ga-OncoFAP to FAP and structurally related members of this family: DPP8 and POP. As reference compounds the FAPI tracer [nat]Ga-FAPI-46, the unselective boronic acid-based inhibitor Talabostat and the highly potent POP inhibitor S 17092 (Suppl. Fig. 1) were analyzed. Experimental IC_{50} values are reported in Table 1. Values for Talabostat and S 17092 were in accordance with literature [19, 20]. The resulting sub-nanomolar binding affinity to human FAP of [nat]Ga-OncoFAP (IC_{50} of 0.51 ± 0.11 nM, n=3) was well in line with reported affinity of other derivatives of OncoFAP [14]. There was a high selectivity for FAP compared to DDP8 (1347-fold) and POP (96-fold). As expected, [nat]Ga-FAPI-46 also displayed high binding potency (IC_{50} of 8.37 ± 0.71 nM, n=3) and selectivity to human FAP compared to DPP8 and POP (> 1000-fold for each). Moreover, our results suggested a superior binding potency (ca. 16-fold) for [nat]Ga-OncoFAP compared to [nat]Ga-FAPI-46. In conclusion, ease of radiosynthesis, metabolic stability, lipophilicity and FAP binding affinity of [nat]Ga-OncoFAP warranted further tracer evaluation in animal models.

Table 1

Inhibition potencies and lipophilicity of [nat]Ga-OncoFAP compared to selected reference compounds and [nat]Ga-FAPI-46. $LogD_{7.4}$ value was determined using the radiolabeled analog. Literature values [19, 20] are displayed in brackets.

Compound	IC_{50} [nM]			$LogD_{7.4}$
	FAP	DPP8	POP	
Talabostat	309 ± 56 (560)	92 ± 5 (4)	n. d. (390)	n. d.
S 17092	n. d.	n. d.	6 ± 3 (K_i: 1.5)	n. d.
[nat]Ga-OncoFAP	0.51 ± 0.11	6870 ± 111	49.20 ± 6.30	-3.91 ± 0.32
[nat]Ga-FAPI-46	8.37 ± 0.71	10.2 ± 3.0 µM	> 10 µM	n. d.

Biodistribution in a murine cancer model

Biodistribution and uptake in tumors were assessed in mice simultaneously bearing subcutaneous human FAP+ and FAP- HT-1080 tumors on the left and right shoulder, respectively (Fig. 2A, B). Gamma counting of harvested organs and tumors 1 h and 3 h after injection of ^{68}Ga-OncoFAP demonstrated strong, specific and temporally stable accumulation in FAP+ tumors with increasing contrast due to fast washout from blood (FAP+ tumor-to-blood ratio 1 h p.i.: 8.6 ± 5.1 (n=6), 3 h p.i.: 38.1 ± 33.1(n=6); ratio FAP+ tumor / FAP- tumor 1 h p.i.: 9.5 ± 5.6, 3 h p.i.: 25.3 ± 19.2). In contrast to other organs liver, kidney

and spleen showed elevated retention at late time points (Suppl. Table 2 & 3). Head-to-head comparison with ^{68}Ga-FAPI-46 revealed significantly higher uptake and tissue-to-blood ratios in FAP+ tumors for ^{68}Ga-OncoFAP 1 h p.i. and comparable uptake between the two tracers 3 h p.i. (uptake in % injected dose/g [% ID/g] 1 h ^{68}Ga-OncoFAP: 2.49 ± 0.56 (n=6), ^{68}Ga-FAPI-46: 1.28 ± 0.40 (n=4), p=.01; tumor-to-blood ratio ^{68}Ga-OncoFAP: 8.61 ± 5.1, ^{68}Ga-FAPI-46: 1.98 ± 0.92, respectively; uptake [% ID/g] 3 h ^{68}Ga-OncoFAP: 2.60 ± 1.96 (n=6), ^{68}Ga-FAPI-46: 2.64 ± 0.60 (n=6), p=.59; tumor-to-blood ratio ^{68}Ga-OncoFAP: 38.06 ± 33.08, ^{68}Ga-FAPI-46: 28.62 ± 17.69, respectively; Suppl. Fig. 4 & 5, Suppl. Table 2 & 3).

In dynamic PET imaging, initial wash in of ^{68}Ga-OncoFAP into FAP+ and FAP- tumors was comparable (Fig. 3A, B); However, the tracer was rapidly washed out of blood, kidney, liver, muscle, spleen and FAP- tumors, whereas it was retained in FAP+ tumors (Fig. 3C) in agreement with results from gamma counting. Thus uptake in FAP+ and FAP- tumors differed significantly from 10 minutes p.i. onwards (6 min: p=.13, 10 min: p=.047, 1 h: p<.001 3 h: p<.001, n=11) and the ratio of uptake between FAP+ and FAP- tumors grew steadily from 1.0 at 4 min p.i. to 1.3 at 10 min p.i., to 5.0 at 1 h p.i., and to 9.3 at 3 h p.i. The uptake after 1 h at FAP+ tumors was significantly higher with ^{68}Ga-OncoFAP as compared to ^{68}Ga-FAPI-46, but not in delayed scanning after 3 h (SUV$_{mean}$ 1 h, ^{68}Ga-OncoFAP: 0.38 ± 0.08 (n=11), ^{68}Ga-FAPI46: 0.25 ± 0.06, (n=10), p=.004; SUV$_{mean}$ 3 h, ^{68}Ga-OncoFAP: 0.21 ± 0.06 (n=5), ^{68}Ga-FAPI46: 0.16 ± 0.06 (n=6), p=.25; Suppl. Fig. 6 & 7, Suppl. Table 5 & 6). Noteworthy, all individual mice that were measured with both tracers (n=9), showed higher ^{68}Ga-OncoFAP than ^{68}Ga-FAPI-46 uptake in FAP+ tumors 1h p.i. independent of the order of measurements (Suppl. Fig. 6C).

Pharmacokinetic modelling using both Patlak analysis and a standard two-tissue compartment model were applied based on VOI-derived ^{68}Ga-OncoFAP PET time-activity curves of muscle, FAP- and FAP+ tumors and an extracorporeally derived AIF. Patlak analysis revealed comparable Patlak intercepts between all three tissues tested. However, the Patlak slope as an indicator of specific binding was significantly different between FAP- and FAP+ tumors (Table 2). Similarly, transfer constants in pharmacokinetic modelling between plasma and the first compartment (k1 and k2), representing passive transfer from blood into tissue, were similar between the tumors. In contrast, transfer constant fraction k3/k4 and the distribution volume (Vs), representing specific tracer binding, were largely and statistically different. The differences in FAP+ tumor uptake comparing ^{68}Ga-OncoFAP with ^{68}Ga-FAPI-46 were also reflected by significantly different Patlak slopes, k3/k4 and Vs confined to FAP+ tumors in between the tracers (geometric mean ± std, Patlak slope ^{68}Ga-OncoFAP: 0.007 ± 0.005 (n=6), ^{68}Ga-FAPI-46: 0.002 ± 0.001 (n=4), p=.02; k3/k4 ^{68}Ga-OncoFAP: 7.9 ± 4.8, ^{68}Ga-FAPI-46: 1.8 ± 2.7, p=.04; Vs ^{68}Ga-OncoFAP: 1.3 ± 0.78, ^{68}Ga-FAPI-46: 0.2 ± 0.29, p=.02; Suppl. Table. 7).

Table 2

Results of pharmacokinetic modelling of dynamic small animal PET using invasive measurements of the arterial input function (AIF) with an extracorporeal circulation and the Twilite measurement unit. A 2-Tissue Compartment Model (2TCM) (k1-k4) and Patlak modelling were applied. Additionally, the k3/k4 ratio and the distribution volume Vs are calculated for 2TCM. Values are displayed as geometric mean ± SD. k1 and k2 demonstrated only small differences between FAP- and FAP+ tumors reflecting similar passive wash in and wash out of tracer. In contrast, k3, k4, k3/k4 and Vs were significantly different between FAP- and FAP+ tumors. This finding establishes specific binding of ^{68}Ga-OncoFAP-DOTAGA only in FAP+ tumors. Consistently, the Patlak model demonstrated unchanged Patlak Intercept, and a significantly different Patlak Slope. No correction of multiple testing was performed due to the strong interdependence of the tested variables.

	Muscle	Tumour FAP-	Tumour FAP+	p-value FAP- vs FAP+
k1	0.071 ± 0.018	0.049 ± 0.010	0.040 ± 0.009	
k2	0.471 ± 0.093	0.331 ± 0.046	0.235 ± 0.034	
k3	0.010 ± 0.022	0.015 ± 0.023	0.062 ± 0.015	
k4	0.026 ± 0.063	0.020 ± 0.032	0.008 ± 0.004	
k3/k4	0.383 ± 3.615	0.740 ± 0.825	7.913 ± 4.825	.002*
Vs	0.058 ± 0.485	0.109 ± 0.140	1.336 ± 0.778	.002*
Patlak Slope	0.000 ± 0.000	0.000 ± 0.000	0.007 ± 0.005	.002*
Patlak Intercept	0.200 ± 0.033	0.216 ± 0.061	0.196 ± 0.074	.59

First time clinical scanning in patients with various cancers

Based on successful targeting of FAP in preclinical tumor models, ^{68}Ga-OncoFAP was applied in clinical imaging in a total of 12 patients with various cancers based on clinical indications. In one patient, whole-body PET/CT was acquired dynamically over 60 minutes (Fig. 4). This patient had a history of bilateral breast cancer and was scanned because of equivocal bilateral axillary lymph node enlargement. The whole-body dynamics displayed rapid clearing of the blood pool and organs over the course of one hour. No uptake was observed in axillary lymph nodes and eventually, lymph node enlargement was clinically judged as benign taking into account all available imaging (PET/CT, MRI and ultrasound). By contrast, ^{68}Ga-OncoFAP accumulated in a previously diagnosed bursitis of the left shoulder, likely reflecting specific tracer binding in the context of inflammatory tissue remodeling (Fig. 4A).

We compared the biodistribution and tumor binding of ^{68}Ga-OncoFAP to a previously published study sample of 19 patients with breast cancer scanned with the FAP ligand ^{68}Ga-FAPI-46 (Table 3) [10]. Patient and acquisition characteristics of the two samples were largely identical besides a higher fraction of

males and a broader spectrum of underlying malignancies in the patients scanned with ^{68}Ga-OncoFAP. Overall, biodistribution was widely comparable between the two tracers; however, ^{68}Ga-OncoFAP showed significantly lower liver uptake (liver SUV_{mean} ^{68}Ga-OncoFAP 0.6 ± 0.2, ^{68}Ga-FAPI-46 0.9 ± 0.3, p<.003). Highly intense ^{68}Ga-OncoFAP and ^{68}Ga-FAPI-46 uptake of the uterus was observed in females (OncoFAP: 17.7 ± 6.3 (n=5), FAPI-46: 11.6 ± 4.5 (n=18), p=.03), probably reflecting fibroblast activation in cyclically changing tissue and in fibroids.

In breast cancer, ^{68}Ga-OncoFAP demonstrated highly intense targeting of primary tumors (SUV_{max}: 12.3 ± 2.3, n=6), lymph node metastases (SUV_{max} 9.7 ± 8.3, n=5) and distant metastases (up to SUV_{max} 19.5) comparable to previously published data on ^{68}Ga-FAPI-46 (Fig. 5, Table 3) [10]. Focal ^{68}Ga-OncoFAP uptake was reliably observed at primary breast cancer lesions, lymph node and distant metastases as depicted in conventional imaging. In addition, ^{68}Ga-OncoFAP-PET identified or substantiated suspicion for additional lesions, e.g. probable lymph node metastases at the internal mammary chain in two patients (Suppl. Fig. 8). Similarly, ^{68}Ga-OncoFAP-PET supported clinical workup of non-breast-cancer patients, e.g. by depicting a peritoneal metastasis of colon cancer (SUV_{max} 20.0), supporting radiation therapy planning in non-FDG-avid fibrosarcoma (SUV_{max} 6.9) and identifying local relapse in post-transplant hepatocellular carcinoma (SUV_{max} 9.7) (Suppl. Fig. 9).

Table 3

Comparison of patient characteristics, acquisition characteristics, SUV_{max} of tumor tissues and other specific uptake sites (e.g. uterus), and SUV_{mean} in blood and non-targeted organs. The study sample of patients scanned with ^{68}Ga-OncoFAP is compared to a previously published study sample scanned at our institution with ^{68}Ga-FAPI-46 . In contrast to the ^{68}Ga-OncoFAP study sample, the ^{68}Ga-FAPI-46 consisted only of female patients with breast cancer. No other significant differences of patient characteristics and imaging characteristics were found. Slight differences of compared SUV could be found between the two tracers. ^{68}Ga-OncoFAP demonstrated higher uptake in the uterus and pancreas, whereas ^{68}Ga-FAPI-46 demonstrated higher uptake in the liver and spleen. However, following Bonferroni correction for multiple testing results (p-value threshold for significance for patient and imaging characteristics of p<.013, and for SUV_{mean} in remaining organs of p<.006) only the hepatic uptake remained statistically different.

Measurement	^{68}Ga-OncoFAP mean ± SD (n=12, if not specified)	^{68}Ga-FAPI-46 mean ± SD (n=19, if not specified) [10]	p-value
age	52 ± 14	49 ± 9	.41
female/male	8/4	19/0	**.009**
weight	74.9 ± 12.3	71.2 ± 14.4	.28
breast cancer /other disease	8/4	19/0	**.009**
whole-body PET/CT / PET/MRI	7/5	9/10	.57
activity [MBq]	163.3 ± 49.5	148.8 ± 47.9	.60
whole-body imaging [min p.i.]	64 ± 18	79 ± 18	.06
breast imaging [min p.i.]	41 ± 31 (n=7)	29 ± 6 (n=18)	.27
primary breast cancer (SUV_{max} breast imaging)	12.3 ± 2.3 (n=6)	14.0 ± 5.7 (n=17)	.86
breast cancer LN metastasis (SUV_{max} whole-body)	9.7 ± 8.3 (n=5)	12.2 ± 6.2 (n=13)	.39
distant metastases any cancer (SUV_{max} whole-body)	14.0 ± 6.7 (n=4)	12.3 ± 0.2 (n=2)	>.99
uterus (SUV_{max} whole-body)	17.7 ± 6.3 (n=5)	11.6 ± 4.5 (n=18)	.03
blood (breast imaging SUV_{mean})	1.6 ± 0.3 (n=7)	1.7 ± 0.2	.32
blood (whole-body SUV_{mean})	1.2 ± 0.2	1.3 ± 0.3	.19
muscle (whole-body SUV_{mean})	1.4 ± 0.5	1.1 ± 0.2	.11
liver (whole-body SUV_{mean})	0.6 ± 0.2	0.9 ± 0.3	**.003**
spleen (whole-body SUV_{mean})	0.8 ± 0.2	1.1 ± 0.8	.02

pancreas (whole-body SUV$_{mean}$)	1.7 ± 0.7	1.1 ± 0.4	.03
bone (whole-body SUV$_{mean}$)	0.6 ± 0.2	0.4 ± 0.1	.09
kidney (whole-body SUV$_{mean}$)	1.5 ± 0.4	1.5 ± 0.4	.72

Discussion

OncoFAP has been recently introduced as a new very high-affinity ligand with striking FAP targeting in small animals upon fluorophore- and ^{177}Lu-labeling [15]. Here, we demonstrate the feasibility of ^{68}Ga-radiolabeling and highly favorable targeting properties in small animal and clinical PET imaging in patients with cancer, validating ^{68}Ga-OncoFAP as a new powerful alternative to clinically established PET tracers.

[68]Ga-labelled clinical PET tracers require a reliable radiosynthesis, high radiochemical yields and high radiochemical purities based on efficient, rapid and simple labelling procedure using state-of-the art equipment. ^{68}Ga-OncoFAP-DOTAGA labelling fulfilled these requirements without reservation on a manual and a fully automated synthesis module. Determined lipophilicity, FAP binding affinity and metabolic stability are ideally suited for whole-body PET imaging justifying its exploration in small animals and clinical translation.

In vivo blocking experiments are traditionally employed to proof specific binding of PET tracers. We employed a different approach of simultaneously implanting individual animals with a FAP-negative and a genetically altered FAP-expressing and otherwise identical tumor line. Accordingly, the observed manyfold difference of uptake between FAP+/FAP- tumor lines can be solely attributed to specific tracer binding. We further substantiated this reasoning by applying pharmacokinetic modelling based on an extracorporeally derived arterial input function. Here, FAP+ and FAP- tumors had similar results for modelling parameters associated with perfusion, permeability and passive retention, whereas parameters reflecting specific target binding were significantly different.

OncoFAP is described as the small organic FAP ligand with the highest affinity [15]. Higher inhibitory activity in a fluorescence-based FAP enzymatic assay for [nat]Ga-OncoFAP compared to [nat]Ga-FAPI-46 substantiates a superior affinity. We benchmarked OncoFAP in head-to-head *in vivo* biodistribution studies against FAPI-46. Again, we observed higher ^{68}Ga-OncoFAP uptake in murine FAP-positive tumors after 1 h in PET imaging and γ-counting. Also, the significant difference between the tracers in pharmacokinetic modelling for parameters k3 and k4 in FAP+/FAP- tumors likely reflects a difference in FAP affinity. Washout characteristics of the two tracers, which are relevant for future theranostic applications, as assessed by the 3 h imaging time point were not found to be statistically different.

Clinical imaging performance of ^{68}Ga-OncoFAP is well in line with prior experience in our center using ^{68}Ga-FAPI-46 [10]. In the group of 12 patients, the tracer reliably bound to primary cancers, lymph node

and distant metastases and is rapidly cleared from unaffected organs. Notably, contrasting the higher-than-expected hepatic uptake in preclinical ^{68}Ga-OncoFAP biodistribution, the only significant difference in tracer uptake was a lower ^{68}Ga-OncoFAP uptake in the liver compared to ^{68}Ga-FAPI-46, rendering relevant hepatic tracer metabolism unlikely at least in humans. Mirroring our recently published results with ^{68}Ga-FAPI-46 in breast cancer [10], ^{68}Ga-OncoFAP-PET imaging led to establish or substantiate novel sites of disease and facilitated work-up in a variety of clinical scenarios. Overall uptake in cancer appeared to be at comparable levels between the tracers in our small study sample.

Our study features limitations. The preclinical head-to-head comparison of ^{68}Ga-OncoFAP with ^{68}Ga-FAPI-46 is based on a small number of tumor bearing mice, that in part redundantly contributed to data for gamma counting, PET quantification and PK-modeling, leading to remaining statistical uncertainties. This explains why we do not overemphasize this comparison. Analysis of clinical translation is retrospective and the number of patients is rather small. The clinical comparison of ^{68}Ga-OncoFAP and ^{68}Ga-FAPI-46 is underpowered and possibly features selection bias.

In conclusion, excellent preclinical and clinical PET imaging characteristics validate ^{68}Ga-OncoFAP as a powerful alternative to currently available FAP tracers. Prospective studies are needed to define its accuracy in relevant clinical scenarios. Moreover, the potential of OncoFAP to deliver therapeutic payloads to cancer requires further preclinical and clinical investigation.

Declarations

Funding

Conflicts of interest/Competing interests

The Department of Nuclear Medicine of the University Hospital of Münster received an institutional research grant from Philochem AG. JM, SC, JM, AG and AZ are employees of Philochem AG, the company that owns and has patented OncoFAP. PB, FG, MB, FB, IA, PD, JC, WR, KS, SH, MW, JT, SW, HB and MS have no other interest to declare.

Availability of data and material

Additional data is available in the supplement.

Code availability (software application or custom code)

Does not apply

Ethics approval (include appropriate approvals or waivers)

Analysis of clinical data has been approved by the Ethics Committee of the Medical Association of Westphalia-Lippe and the Medical Faculty of the University of Münster (Az. 2021-408-f-S).

Consent to participate (include appropriate statements)

All patients gave written informed consent for ^{68}Ga-OncoFAP-PET/CT and/or PET/MRI imaging and retrospective scientific analysis.

Consent for publication

Not necessary, as no potential identifying details / images are published.

Acknowledgements

References

1. Kratochwil C, Flechsig P, Lindner T, Abderrahim L, Altmann A, Mier W, et al. 68Ga-FAPI PET/CT: Tracer Uptake in 28 Different Kinds of Cancer. J Nucl Med. 2019;60:801–5.

2. Garin-Chesa P, Old LJ, Rettig WJ. Cell surface glycoprotein of reactive stromal fibroblasts as a potential antibody target in human epithelial cancers. Proc National Acad Sci. 1990;87:7235–9.

3. Yazbeck R, Jaenisch SE, Abbott CA. Potential disease biomarkers: dipeptidyl peptidase 4 and fibroblast activation protein. Protoplasma. 2018;255:375–86.

4. Giesel FL, Kratochwil C, Lindner T, Marschalek MM, Loktev A, Lehnert W, et al. 68Ga-FAPI PET/CT: Biodistribution and Preliminary Dosimetry Estimate of 2 DOTA-Containing FAP-Targeting Agents in Patients with Various Cancers. J Nucl Med. 2019;60:386–92.

5. Loktev A, Lindner T, Mier W, Debus J, Altmann A, Jäger D, et al. A Tumor-Imaging Method Targeting Cancer-Associated Fibroblasts. J Nucl Med. 2018;59:1423–9.

6. Lindner T, Loktev A, Altmann A, Giesel F, Kratochwil C, Debus J, et al. Development of Quinoline-Based Theranostic Ligands for the Targeting of Fibroblast Activation Protein. J Nucl Med. 2018;59:1415–22.

7. Röhrich M, Naumann P, Giesel FL, Choyke PL, Staudinger F, Wefers A, et al. Impact of 68Ga-FAPI PET/CT Imaging on the Therapeutic Management of Primary and Recurrent Pancreatic Ductal Adenocarcinomas. J Nucl Med. 2021;62:779–86.

8. Guo W, Pang Y, Yao L, Zhao L, Fan C, Ke J, et al. Imaging fibroblast activation protein in liver cancer: a single-center post hoc retrospective analysis to compare [68Ga]Ga-FAPI-04 PET/CT versus MRI and [18F]-FDG PET/CT. Eur J Nucl Med Mol I. 2021;48:1604–17.

9. Pang Y, Zhao L, Luo Z, Hao B, Wu H, Lin Q, et al. Comparison of 68Ga-FAPI and 18F-FDG Uptake in Gastric, Duodenal, and Colorectal Cancers. Radiology. 2020;298:203275.

10. Backhaus P, Burg MC, Roll W, Büther F, Breyholz H-J, Weigel S, et al. Simultaneous FAPI PET/MRI Targeting the Fibroblast-Activation Protein for Breast Cancer. Radiology. 2021; Oct 12:204677. doi: 10.1148/radiol.2021204677

11. Strosberg J, El-Haddad G, Wolin E, Hendifar A, Yao J, Chasen B, et al. Phase 3 Trial of 177Lu-Dotatate for Midgut Neuroendocrine Tumors. New Engl J Medicine. 2017;376:125–35.

12. Sartor O, Bono J de, Chi KN, Fizazi K, Herrmann K, Rahbar K, et al. Lutetium-177−PSMA-617 for Metastatic Castration-Resistant Prostate Cancer. New Engl J Med. 2021;

13. Baum RP, Schuchardt C, Singh A, Chantadisai M, Robiller FC, Zhang J, et al. Feasibility, Biodistribution and Preliminary Dosimetry in Peptide-Targeted Radionuclide Therapy (PTRT) of Diverse Adenocarcinomas using 177Lu-FAP-2286: First-in-Human Results. J Nucl Med. 2021;jnumed.120.259192.

14. Ferdinandus J, Costa PF, Kessler L, Weber M, Hirmas N, Kostbade K, et al. Initial clinical experience with 90 Y-FAPI-46 radioligand therapy for advanced stage solid tumors: a case series of nine patients. J Nucl Med. 2021;jnumed.121.262468.

15. Millul J, Bassi G, Mock J, Elsayed A, Pellegrino C, Zana A, et al. An ultra-high-affinity small organic ligand of fibroblast activation protein for tumor-targeting applications. Proc National Acad Sci. 2021;118:e2101852118.

16. Meyer C, Dahlbom M, Lindner T, Vauclin S, Mona C, Slavik R, et al. Radiation Dosimetry and Biodistribution of 68Ga-FAPI-46 PET Imaging in Cancer Patients. J Nucl Med. 2020;61:1171–7.

17. Prante O, Hocke C, Löber S, Hübner H, Gmeiner P, Kuwert T. Tissue distribution of radioiodinated FAUC113: assessment of a pyrazolo(1,5-a) pyridine based dopamine D4 receptor radioligand candidate. Nuklearmedizin Nucl Medicine. 2006;45:41–8.

18. Backhaus P, Büther F, Wachsmuth L, Frohwein L, Buchholz R, Karst U, et al. Toward precise arterial input functions derived from DCE-MRI through a novel extracorporeal circulation approach in mice. Magnet Reson Med. 2020;84:1404–15.

19. Lawandi J, Gerber-Lemaire S, Juillerat-Jeanneret L, Moitessier N. Inhibitors of Prolyl Oligopeptidases for the Therapy of Human Diseases: Defining Diseases and Inhibitors. J Med Chem. 2010;53:3423–

38.

20. Lankas GR, Leiting B, Roy RS, Eiermann GJ, Beconi MG, Biftu T, et al. Dipeptidyl Peptidase IV Inhibition for the Treatment of Type 2 Diabetes: Potential Importance of Selectivity Over Dipeptidyl Peptidases 8 and 9. Diabetes. 2005;54:2988–94.
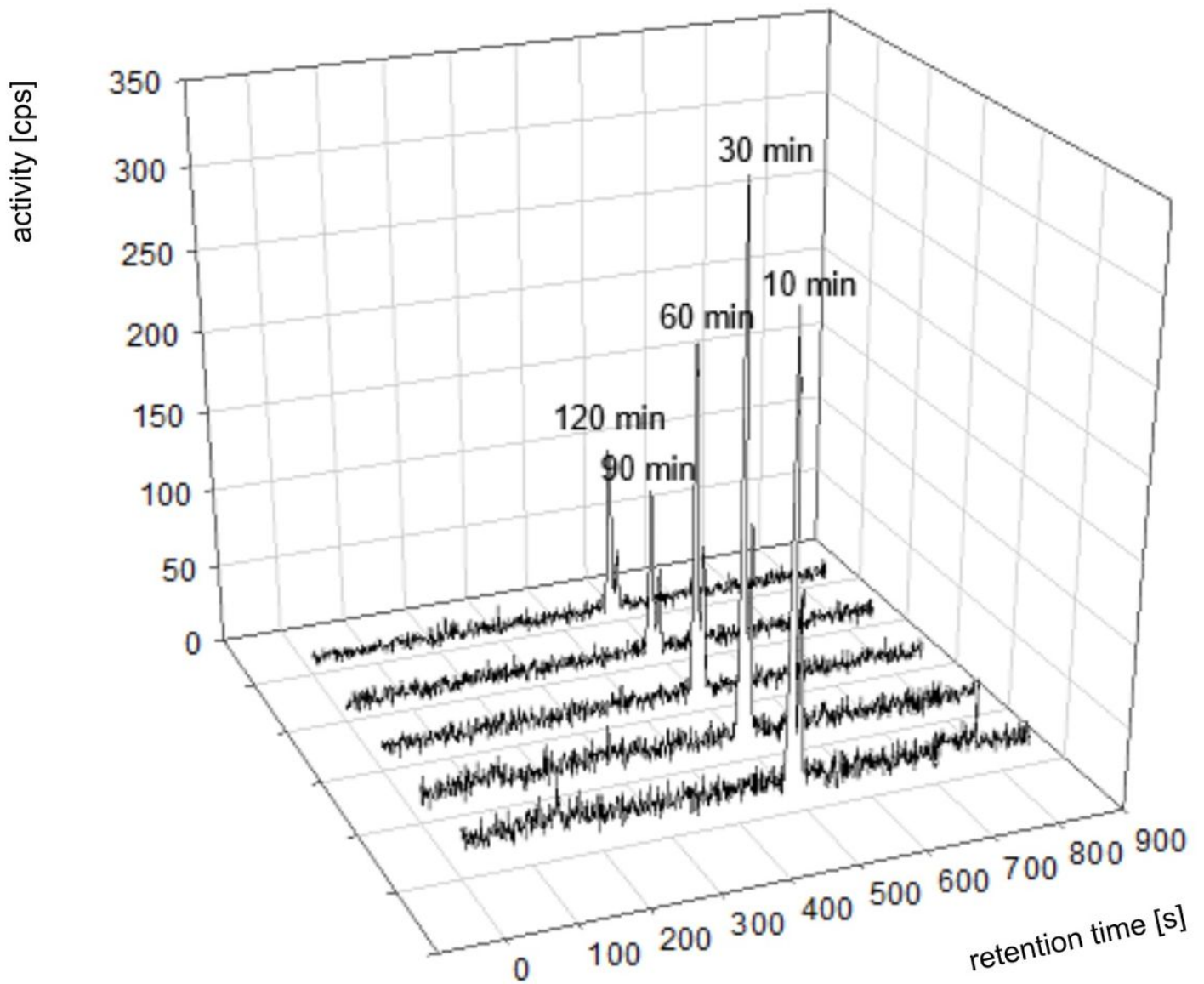
Figures

Figure 1

Stability of [68Ga]Ga-OncoFAP-DOTAGA in human blood serum at 37 °C as analyzed by analytical radio-HPLC. Radio-HPLC chromatograms are shown for incubation times from 10 to 120 min. See suppl. fig. 3 for murine serum stability.
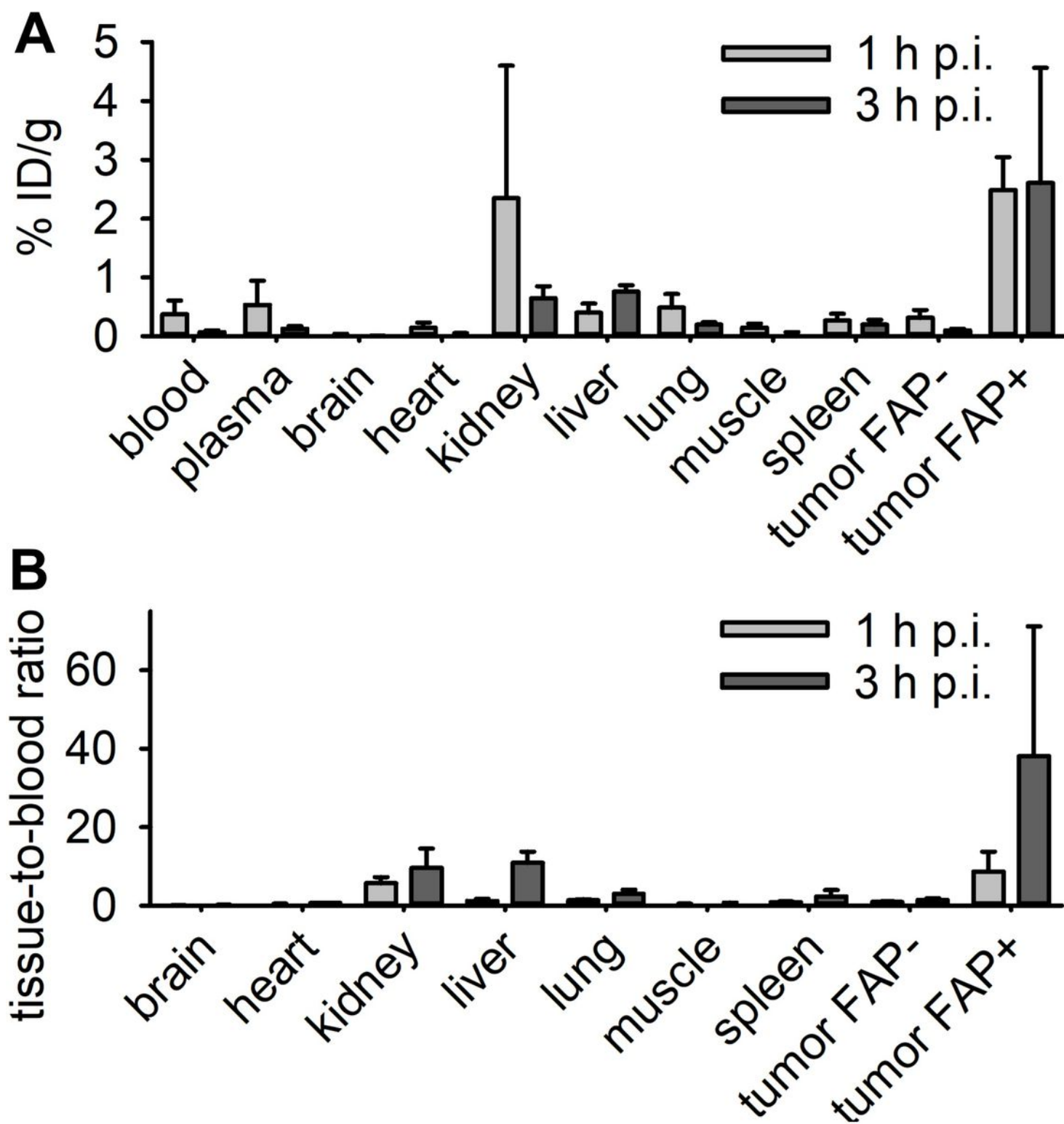
Figure 2

(A) Results from gamma counting in % injected dose per g (% ID/g) of organs harvested 1 h and 3 h after i.v. injection of 68Ga-OncoFAP, and (B) tissue-to-blood ratios in mice bearing subcutaneous HT1080 (left shoulder, FAP-) and HT1080-hFAP (right shoulder, FAP+) tumors (6 mice for each time point). 68Ga-OncoFAP demonstrated strong and selective tumor accumulation in FAP+ tumors. In contrast to blood and FAP- tumors, accumulation persisted in FAP+ tumors from 1 to 3 h resulting in incrementing binding

ratios. 3 h p.i. only trace uptake remained in blood and most organs except for the liver, kidney and spleen. See suppl. table 2 – 4 and suppl. fig. 4 & 5 for all gamma counting data.
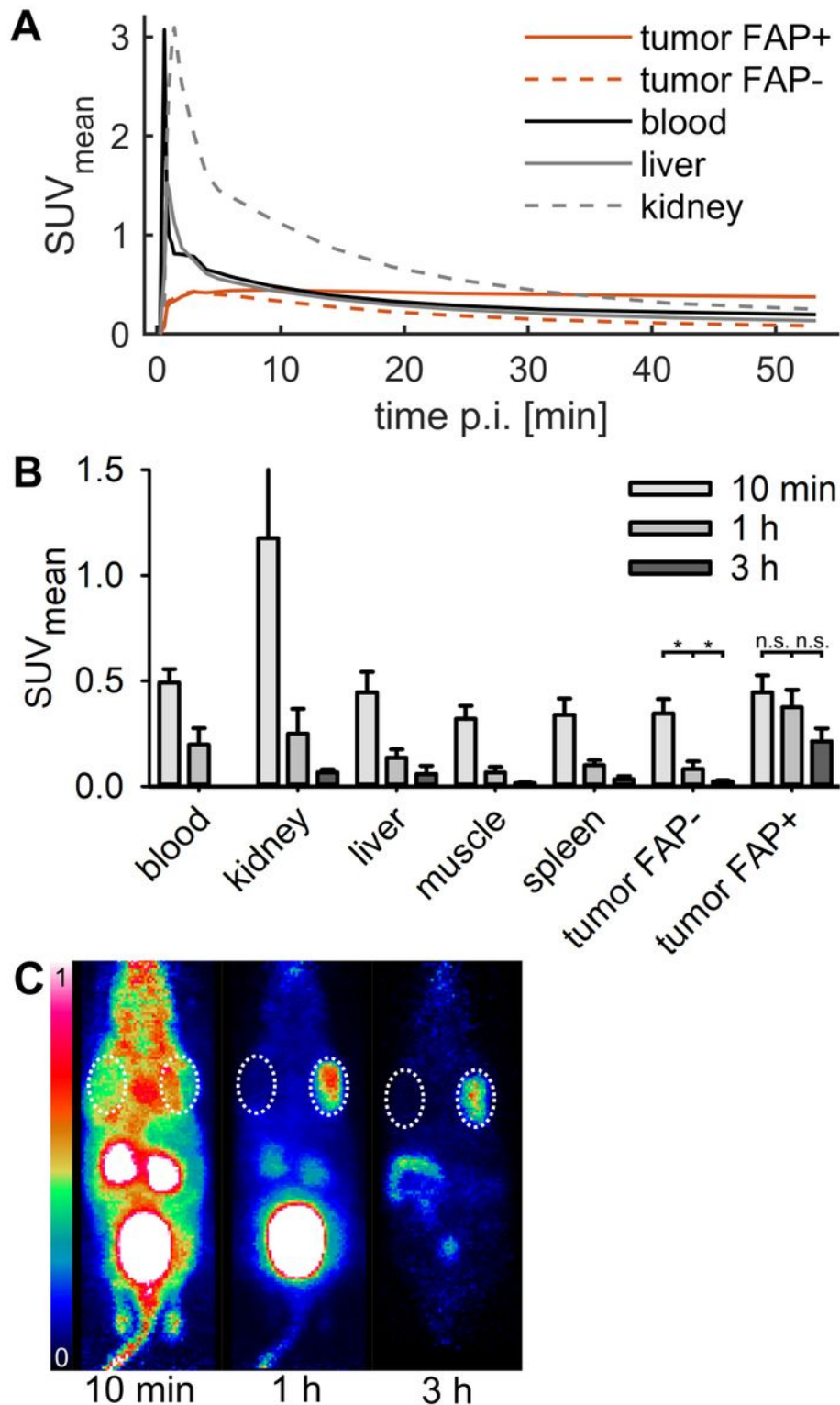

Figure 3

Results from dynamic PET of mice (11 mice, 0-60 min p.i. of 68Ga-OncoFAP) bearing subcutaneous HT1080 (left shoulder, FAP-) and HT1080-FAP (right shoulder, FAP+) tumors. Of these, 5 were additionally measured 3 h p.i. (A) Mean time activity curves of 11 mice. (B) Uptake in organs and tumors 10 min

(n=11), 1 h (n=11) and 3 h p.i. (n=5), with significantly different results for FAP negative tumors (10 min: 0.35 ± 0.07, 1 h: 0.08 ± 0.04, 3 h: 0.02 ± 0.01, 10 min vs 1 h: p <.001, 1 h vs 3 h: p <.001) and non-significantly different values for FAP positive tumors (10 min: 0.45 ± 0.08, 1 h: 0.38 ± 0.08, 3 h: 0.21 ± 0.06, 10 min vs 1 h: p=.09, 1 h vs 3 h: p=.055). The whisker of 10 minute kidney activity is truncated to better display the activity range of the remainder of organs /materials. See suppl. table 5 & 6 and suppl. fig. 6 & 7 for all PET measurement data. (C) Example mouse PET maximum intensity projection (MIP) 10 min, 1 h and 3 h p.i. scaled to SUV 0-1. FAP- (left shoulder, left in image) and FAP+ (right shoulder, right in image) tumors are highlighted.
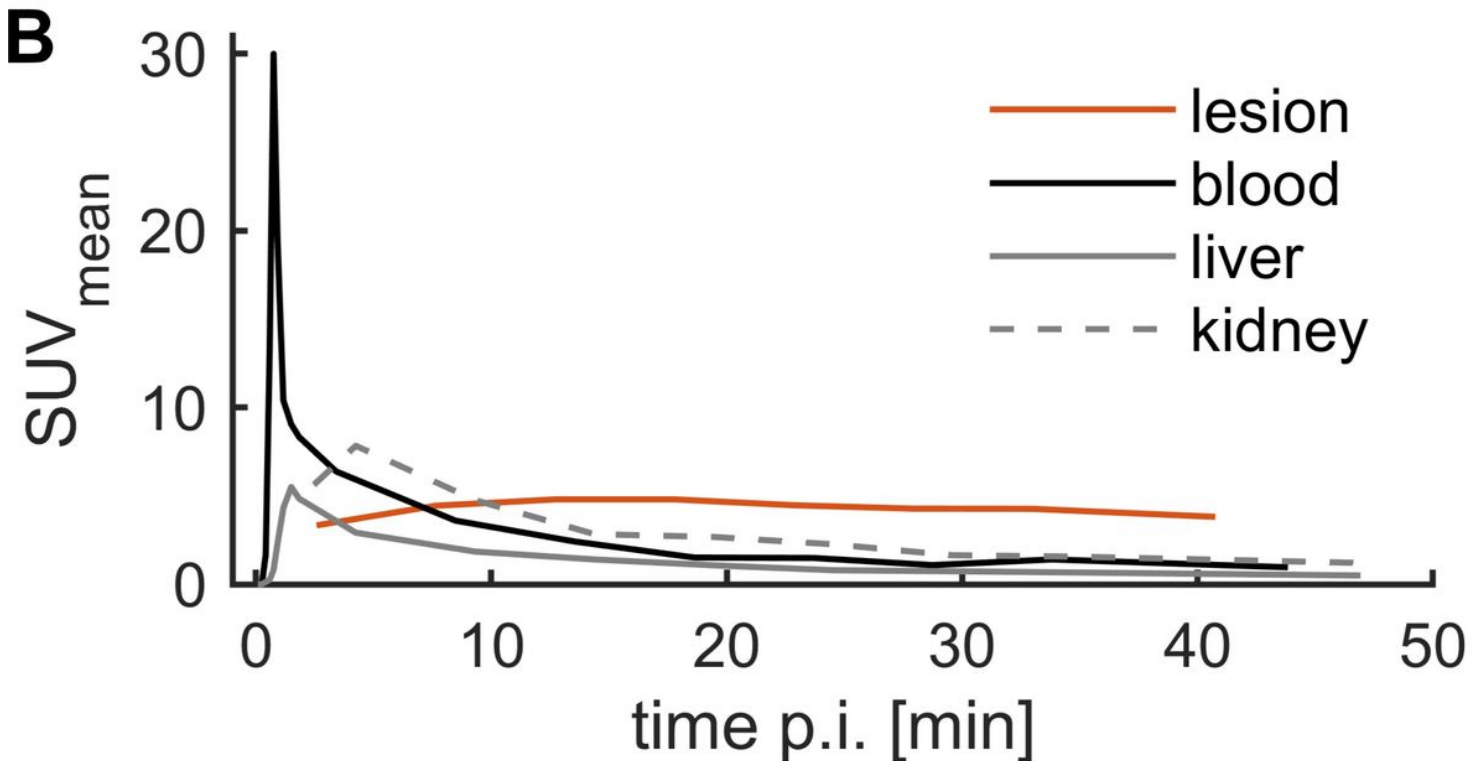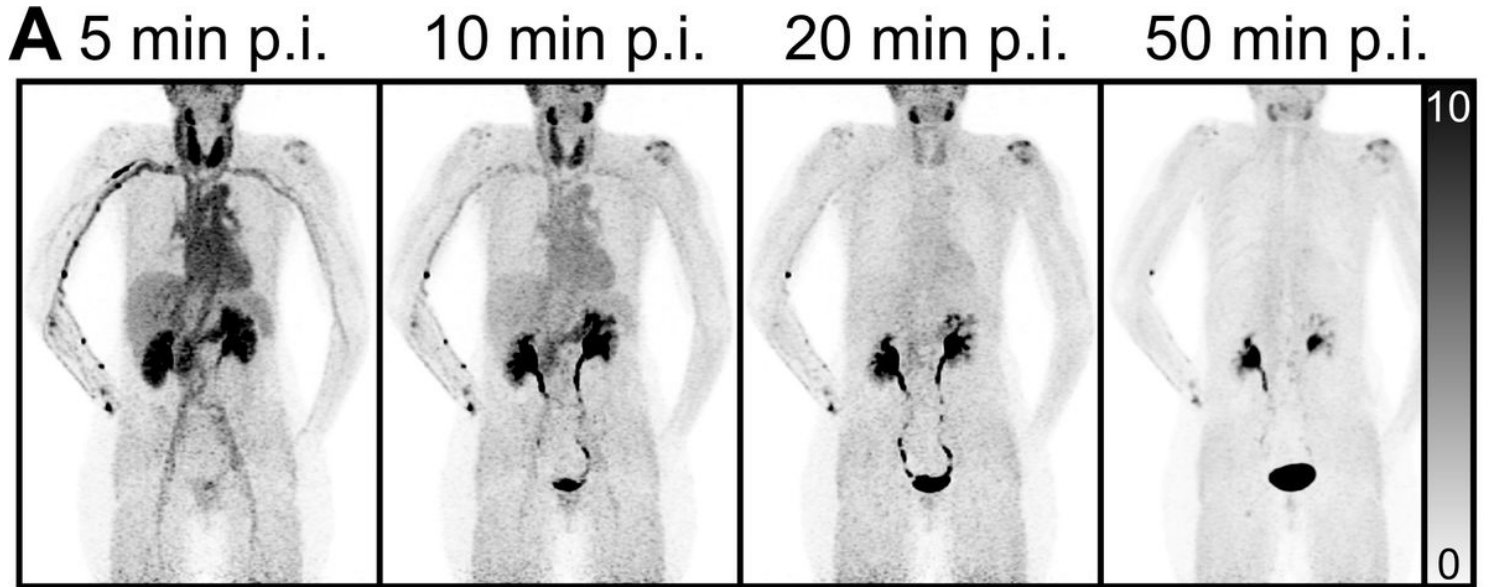

Figure 4

Results from a 60-min whole-body dynamic 68Ga-OncoFAP-PET/CT in a female patient. This patient had a history of bilateral breast cancer and was examined for bilateral intermediate axillary lymph node enlargement. Enlarged lymph nodes showed no 68Ga-OncoFAP uptake and eventually no recurrence was established. Patient had bursitis of the left shoulder as a secondary finding. The shoulder demonstrated strong tracer uptake that persisted over time, whereas tracer washed out rapidly from organs. (A) maximum intensity projections (MIP) 5, 10, 20 and 50 min p.i. (rounded). MIPs are adjusted to SUV 0-10. (B) Time activity curves (TAC) of VOIs of left shoulder lesion (bursitis), blood, liver and kidney.
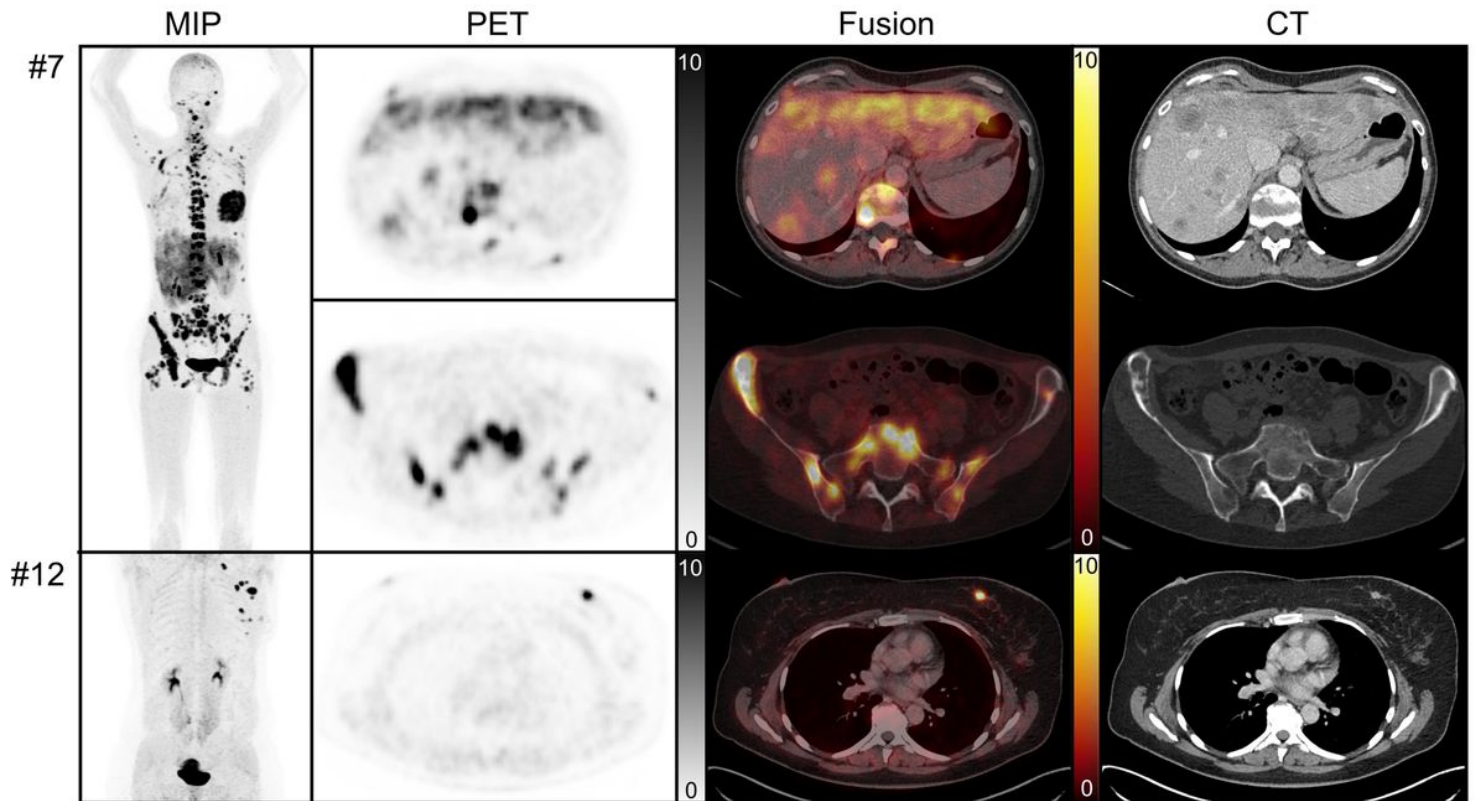

Figure 5

Two example patients scanned with 68Ga-OncoFAP. Patient #7 with newly disseminated metastatic disease to lymph nodes, bones and liver at primary diagnosis of locally advanced breast cancer. Whole-body maximum intensity projection (MIP) PET, fusion and contrast-enhanced CT are shown in a slice at the liver and the pelvis demonstrating osseous (SUVmax 19.5) and hepatic metastases (SUVmax 9.9). Patient #12 with newly diagnosed breast cancer metastatic to local and supraclavicular lymph nodes. MIP, PET, fusion and contrast enhanced CT are shown in a slice at the breast demonstrating strong uptake of even sub-centimeter breast lesions (SUVmax 15.1). All PET images are adjusted to SUV 0-10.

Supplementary Files

This is a list of supplementary files associated with this preprint. Click to download.

- Scheme1.tif

- Supplement.docx